Thermodynamics and Kinetics of the Solid Solution of HNO_3 in Ice

Emmanuel Thibert and Florent Dominé*

CNRS, Laboratoire de Glaciologie et Géophysique de l'Environnement, and Université Joseph Fourier, BP 96, 38402 Saint Martin d'Hères Cedex, France

Received: December 18, 1997; In Final Form: March 3, 1998

The diffusion and solubility of gaseous HNO_3 in ice have been measured as a function of temperature and HNO_3 partial pressure between −8 and −35 °C. The diffusion coefficient of HNO_3 follows the Arrhenius expression $D = 1.37 \times 10^{-2610/T}$ cm^2 s^{-1}, but these values probably represent upper limits because of the existence of diffusion short circuits. The solubility of HNO_3 in ice, X^0_{HNO3}, is about 5×10^{-7} mole fraction at −15 °C and $P_{HNO_3} = 10^{-3}$ Pa, and its temperature and partial pressure dependences are $X^0_{HNO3} = 2.37 \times 10^{-12}\ e^{(3532.2/T)}(P_{HNO_3})^{1/2.3}$ mole fraction, where P_{HNO_3} is the HNO_3 partial pressure in Pa, and T is the temperature in Kelvin. These solubility data have been used to build the partial pressure versus inverse temperature phase diagram and to calculate the *solidus* of the temperature−composition phase diagram and the ice-to-water partition coefficient K. K varies with temperature between 3×10^{-6} and 1.6×10^{-5}. Implications for ice cloud chemistry and for the interpretation of ice core analyses are briefly discussed.

I. Introduction

I.1. Objectives. Gaseous HNO_3 is involved in numerous atmospheric processes such as acid rain,[1] photochemical smog,[2] and the condensation of polar stratospheric clouds involved in ozone depletion.[3] HNO_3 is also a key step in the atmospheric phase of the geochemical nitrogen cycle. Tropospheric HNO_3 is produced by anthropogenic and natural sources. The most important anthropogenic source is fossil fuel combustion, where atmospheric N_2 is dissociated, thus forming NO, which is subsequently oxidized to HNO_3 in the atmosphere. Natural sources include biomass burning, lightning, and biomass and soil emissions.[4,5] In the stratosphere, the natural source of HNO_3 is N_2O photooxidation. N_2O is produced by various sources that include microbial processes in soils and natural waters. Because it is inert in the troposphere, its lifetime in the troposphere is long enough to allow diffusion to the stratosphere.[6]

HNO_3 is a strong acid and readily dissolves in atmospheric water. It has also been found in snow,[7] where it is detected as the nitrate ion, NO_3^-, by ion chromatography. The presence of NO_3^- in snow suggests that the interactions between HNO_3 and ice will deplete the gas phase in HNO_3, and the mechanism of incorporation of HNO_3 in ice forming in the atmosphere must then be studied to understand ice cloud chemistry. NO_3^- is retained to variable extents in ice after its deposition on the ground, and the variations with depth of the nitrate ion in ice cores are thought to be linked to past variations in the nitrogen cycle.[8] The study of the various interactions of HNO_3 with ice is therefore also necessary to reconstruct past atmospheric HNO_3 concentrations from ice core analyses.[9]

Dominé and co-workers[10,11] have studied the mechanism of incorporation of HCl and HNO_3 in ice. It is believed that the composition of new crystal layers on ice growing from the gas phase is determined by condensation kinetics, where the sticking coefficients of H_2O and the acid are key parameters. Equilibration by solid-state diffusion then tends to drive the ice composition toward thermodynamic equilibrium with the atmosphere. The diffusion coefficient and the equilibrium solubility of HNO_3 in ice must therefore be known to understand quantitatively the amount of HNO_3 incorporated in growing ice.

In a manner similar to what has been done for HCl,[12,13] we have then measured the thermodynamics and the kinetics of the solid solution of HNO_3 in ice between −8 and −35 °C. The kinetic results obtained are used to derive an Arrhenius expression for the diffusion coefficient. The thermodynamic results are used to derive the partial pressure vs inverse temperature phase diagram, as well as the solidus curve of the more commonly used temperature vs composition phase diagram.

I.2. Previous Studies. The first studies dedicated to the HNO_3/H_2O temperature−composition phase diagram have focused on crystallization points. Pickering[14] found the existence of two hydrates: the nitric acid trihydrate, $HNO_3 \cdot 3H_2O$, and the nitric acid monohydrate $HNO_3 \cdot H_2O$. Those results were later confirmed by Kuster and Kremann[15] and Biltz et al.[16] In 1956, Potier and Potier[17] determined the existence of a new hydrate, the nitric acid quaterhydrate ($HNO_3 \cdot {}^1/_4H_2O$).

Further studies have been performed after the discovery of the ozone hole and the awareness that polar stratospheric clouds were key steps in ozone depletion. The chemical composition of the particles forming these clouds was at that time uncertain and has therefore motivated numerous laboratory studies. However, the solid phase in equilibrium with the gas phase under the temperature and HNO_3 partial pressure (T, P_{HNO_3}; see Table 1 for the meaning of symbols) conditions encountered in the polar stratosphere (typically $T = 190$ K, $P_{HNO_3} = 10^{-5}-10^{-4}$ Pa, and $P_{H_2O} = 10^{-2}$ Pa) is expected to be nitric acid trihydrate.[18−20] Therefore, most of those recent laboratory studies were devoted to the composition range 0.1−0.5 HNO_3 mole fraction and focused neither on the composition of HNO_3 solid solutions in ice nor on the *solidus* composition.

Recently, Ji and Petit[21] have closely examined the temperature−composition phase diagram by differential scanning

* To whom correspondence should be addressed. E-mail: florent@glaciog.ujf-grenoble.fr.

S1089-5647(98)00569-0 CCC: $15.00
Published on Web 05/12/1998

TABLE 1: Symbols

symbol	definition
D	diffusion coefficient of HNO_3 in ice ($cm^2\ s^{-1}$)
D'	diffusion coefficient of HNO_3 in small-angle boundaries ($cm^2\ s^{-1}$)
D_{app}	apparent diffusion coefficient resulting from the simultaneous diffusion in bulk ice and in small-angle boundaries ($cm^2\ s^{-1}$)
E_{diff}	activation energy of diffusion of HNO_3 in ice (kJ/mol)
P_{HNO_3}	partial pressure of HNO_3 (Pa)
T	temperature (K)
$X^0_{HNO3}(T, P_{HNO_3})$	equilibrium mole fraction of HNO_3 in ice
$S(T)$	saturation solubility of HNO_3 in ice, i.e. X^0_{HNO3} on the solidus line
K	solid-to-liquid partition coefficient
n	ice vapor pressure depression factor
Δh^s_{HNO3}	partial molar enthalpy of sublimation of HNO_3 from ice (kJ/mol)
Δh^v_{HNO3}	partial molar enthalpy of vaporization of HNO_3 from water (kJ/mol)

calorimetry and demonstrated the existence of the nitric acid dihydrate, $HNO_3{\cdot}2H_2O$. This result confirms the hypothesis proposed by Tolbert and Middelbrook[22] and Ritzhaupt and Devlin[23] to explain their infrared spectra of solid HNO_3/H_2O films. Koehler et al.[24] have also confirmed the composition of this hydrate with a mass spectrometry analysis performed during its sublimation. Laird and Sommerfeld[25] have studied the adsorption of HNO_3 on ice. Exposing ice with high surface area to an HNO_3 partial pressure of 2×10^{-4} Pa at -20 °C, the authors observed the formation of a new phase that they identified as nitric acid trihydrate.

To determine the composition of the solid solution of HNO_3 in ice as a function of T and P_{HNO_3}, we have applied the method that has been previously used for HCl.[12,13] Preliminary data at -15 °C have shown that the equilibrium solubility of HNO_3 in ice is much lower than that of HCl.[11,26,27] New results have now been obtained at four temperatures between -8 and -35 °C so that we have been able to build a P_{HNO_3} versus $1/T$ phase diagram. We then use this phase diagram to attempt to predict the HNO_3 mole fraction in cirrus clouds and in condensation trails of airplanes.

II. Experimental Section

The experimental method used to measure HCl diffusion and solubility in ice has already been described in detail.[13] Since most of this experimental procedure was also applied for HNO_3, only a brief summary will be given here. We used cylindrical pure ice single crystals with their $\vec{c}$ axis parrallel to the axis of the cylinder, which were grown by a modified Bridgman method. These crystals, 8 cm in diameter, were cut to a length of 3−5 cm, placed in a stainless steel diffusion chamber and exposed to the desired partial pressure of HNO_3, which was obtained by flowing laboratory-made gas mixtures of HNO_3 diluted in water−saturated nitrogen over the ice sample. Because of its thermal and photochemical instability,[28] gaseous HNO_3 was synthesized in the laboratory before each diffusion experiment by the action of sulfuric acid (99% pure) on sodium nitrate (99,9% pure) according to

$$H_2SO_4 + 2NaNO_3 \rightarrow 2HNO_3 + Na_2SO_4 \qquad (1)$$

Gaseous HNO_3 produced by reaction 1 was cryotrapped at 77 K to form solid HNO_3. Condensed HNO_3 was evaporated in a gas handling system to make diluted mixtures in nitrogen. To control the purity of our nitric acid and the dilution rates of gaseous mixtures, HNO_3 partial pressure was measured by UV absorption at 213.9 nm. The partial pressure was calculated with the Beer−Lambert law and the absorption cross section of HNO_3 at 213.9 nm and 298 K using the value of Burkholder et al.,[29] which is 4.32×10^{-19} cm^2/molecule.

After a diffusion time of 1−4 weeks, the samples were sliced on a lathe in a cold room in 25 μm thick sections to a depth of 1−2 mm. The collected shavings were melted, diluted in water, and analyzed by ion chromatography where HNO_3 was detected as the nitrate ion. Diffusion profiles were fitted to the solution to Fick's laws of diffusion in a semi-infinite solid with a constant supply of the diffusing species, which is[30]

$$X_{HNO_3}(x, t) = X^0_{HNO_3}(T, P_{HNO_3})\left[1 - \mathrm{erf}\left(\frac{x}{2\sqrt{Dt}}\right)\right] \qquad (2)$$

where X_{HNO_3} is the HNO_3 mole fraction at a distance x from the surface after a diffusion time t, $X^0_{HNO_3}$ is the equilibrium solubility (mole fraction) of HNO_3 in ice under the (T, P_{HNO_3}) conditions of the experiment, D is the diffusion coefficient, and *erf* is the error function. As explained for HCl,[12,13] small-angle boundaries present in ice crystals act as diffusion short circuits. HCl diffusion profiles therefore showed some deviation from eq 2 at distances far from the surface ($x > 200$ μm). This was also observed for HNO_3 diffusion profiles but to a much lesser extent. The deviation was significant only at deeper slices, typically 300 μm rather than 200 μm for HCl.[12] Thus, as done for HCl, eq 2 was only used in the first part of the HNO_3 diffusion profile, which is little affected by short circuits.[31] Typically, five to seven data points were used for each fit, which is a larger number than for HCl. Because of the occurrence of diffusion short circuits, values of D determined here are, as for HCl, somewhat overestimated and must therefore be considered as upper limits. Uncertainties in the determination of the solubility and diffusion coefficient from eq 2 have been estimated from: (a) the analytical error in the chromatograph calibration and the variations in the blank levels (analytical error) and (b) the position of the cutting tool during the lathing procedure. The detection limit for HNO_3 concentration in diffusion profiles is 8×10^{-9} mole fraction. The error of the diffusion coefficient and of the solubility has been estimated at 60% (not taking into account the accelerating effect of diffusion short circuits, as detailed below) and 20%, respectively.[13]

III. Results

We have obtained 18 diffusion profiles under 10 different (T, P_{HNO_3}) conditions, whose data are summarized in Table 2.

III.1. Kinetics of Diffusion. A typical diffusion profile, and the fit to eq 2 of the first six data points, is shown in Figure 1. The values of D measured for HNO_3 at -8 and -15 °C have been plotted in an Arrhenius form in Figure 2. An Arrhenius law is expected for a diffusion coefficient if the temperature dependences of the enthalpy and entropy of difusion are small and if only one mechanism of diffusion is involved.[30] The D values measured here are 1−2 orders of magnitude higher than those measured by us for HCl.[13] Because the values obtained for HCl were affected by small-angle boundaries that acted as diffusion short circuits and because short circuit densities can vary among different ice samples, D_{HCl} values did not follow an Arrhenius law.[13] HNO_3 diffusion profiles are also affected by short circuits, but to a smaller extent, and Figure 1 shows that D appears to follow an Arrhenius law. Because D values must be considered as upper limits, the Arrhenius parameters were determined using only the lowest values obtained for each

TABLE 2: Experimental Results of the Diffusion of Gaseous HNO_3 in Ice between −8 and −35 °C

exp no.	1	2	3	4	5	6	7	8	9
temp (°C)	−8	−8	−15	−15	−15	−15	−15	−15	−25
direction relative to the $\vec{c}$ axis	||[a]	⊥[b]	||[a]	||[a]	⊥[b]	||[a]	||[a]	⊥[b]	⊥[b]
P_{HNO_3} (10^{-3} Pa)	1.28	1.28	8.56	4.3	4.3	1.06	0.534	0.534	4.29
diffusion time[c] (10^6 s)	0.59	0.59	0.58	0.58	0.58	1.14	1.27	1.27	1.29
solubility $X_{HNO_3} \times 10^6$ (mole fraction)[d]	0.670	0.719	2.86	2.25	2.0	1.44	0.831	0.987	3.89
diffusion coefficient (10^{-12} cm^2/s)	223	261	110	76	84	112	97	109	46
exp no.	10	11	12	13	14	15	16	17[e]	18[e]
temp (°C)	−25	−25	−25	−35	−35	−8	−8	−35[e]	−35[e]
direction relative to the $\vec{c}$ axis	||[a]	⊥[b]	||[a]	⊥[b]	||[a]	||[a]	⊥[b]	||[a]	⊥[b]
P_{HNO_3} (10^{-3} Pa)	4.29	0.716	0.716	0.618	0.618	0.426	0.426	2.13	2.13
diffusion time[c] (10^6 s)	1.29	1.63	1.63	0.83	0.83	0.83	0.83	1.33	1.33
solubility $X_{HNO_3} \times 10^6$ (mole fraction)[d]	3.23	1.63	1.7	2.73	2.41	0.529	0.48	4.68	4.02
diffusion coefficient (10^{-12} cm^2/s)	57	69	63	11	19	247	235	31[c]	25[c]

[a] The direction of diffusion is parallel to the $\vec{c}$ axis. [b] The direction of diffusion is normal to the $\vec{c}$ axis. [c] 10^6 s ≈ 11.6 days. [d] HNO_3 mole fraction $10^{-7} \approx 5 \times 10^{-6}$ mol/L of ice at 0 °C. [e] No annealing after machining and prior to doping.

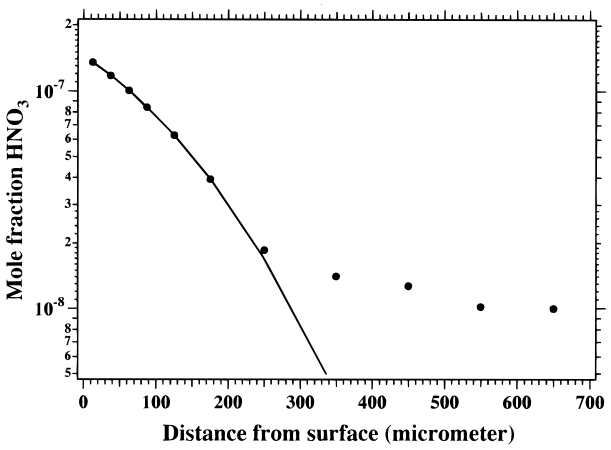

Figure 1. Typical diffusion profile of HNO_3 in ice. The fit to eq 2, using the first six data points, is shown. Other points are affected by diffusion in small-angle boundaries. Experimental conditions are $T = -15$ °C, $P_{HNO_3} = 1.06 \times 10^{-3}$ Pa, $t = 1.14 \times 10^6$ s (13.2 days).

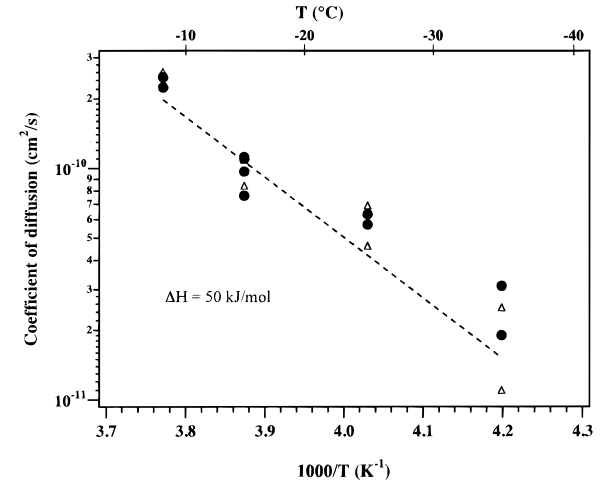

Figure 2. Arrhenius plot of the diffusion coefficient of HNO_3 in ice, $D_{app.}$ These values follow an Arrhenius law with an activation energy of 50 kJ/mol, which suggests that $D \approx D_{app}$.

crystallographic direction at each temperature. The resulting Arrhenius expression, derived from eight values and shown in Figure 1, is (with T in K)

$$D = 1.37 \times 10^{-2610/T} \text{ cm}^2 \text{ s}^{-1} \quad (3)$$

The activation energy of diffusion deduced from this value is $E_{diff} = 50$ kJ/mol. Using the lowest D value at each temperature, regardless of crystallographic orientation, yields $E_{diff} = 54.6$ kJ/mol. Using the lowest values orthogonal to the $\vec{c}$ axis yields $E_{diff\perp} = 56.2$ kJ/mol. Using the lowest values parallel to the $\vec{c}$ axis yield $E_{diff||} = 43.6$ kJ/mol. Considering the small anisotropy of diffusion observed for H_2O (ref 32) and HCl[13] in ice, our preferred value is that of eq 3, because it probably minimizes errors. The error on a single D value is 60%, but this does not take into account the effect of short circuits and the variation of their density. Because the effect of short circuits is not quantified, it is not possible to evaluate the absolute error of the parameters of eq 3, which yield upper limits of D and should be considered as a preliminary expression.

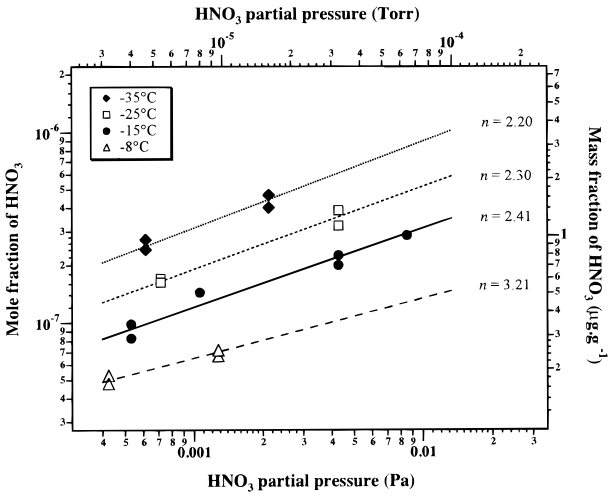

Figure 3. Equilibrium solubility of HNO_3 in ice (in mole fraction and in mass fraction) as a function of the partial pressure of HNO_3, P_{HNO_3}. For each temperature, the data have been fitted to eq 4.

III.2. Thermodynamics. The equilibrium solubility of HNO_3 in ice has been reported in Figure 3 as a function of P_{HNO_3} for each of the four temperatures investigated. As proposed by Hanson and Mauersberger[18] and demonstrated for HCl by Thibert and Dominé,[13] the partial pressure of HNO_3 over the solid solution can be related to the solubility $X^0_{HNO_3}$ by the relation

$$P_{HNO_3} = A(T)(X^0_{HNO_3})^n \quad (4)$$

where $A(T)$ is a coefficient that depends only on temperature T and n is the ice vapor pressure depression factor, which corresponds to the number of entities associated with the incorporation of HNO_3 in ice. $A(T)$ is related to the partial molar enthalpy of sublimation of HNO_3 from the solid solution,

TABLE 3: Determination of the Three Parameters A_0, Δh^s_{HNO3}, and n According to the Two Methods

	A_0 (Pa)	$\Delta h^s_{HNO_3}$ (kJ/mol)	n
separate linear regressions	$(5.47 \pm 1.3) \times 10^{26}$	67.5 ± 8.9	2.30 ± 0.1
three-variables method	1.32×10^{27}	68.9	2.32

$\Delta h^s_{HNO_3}$, so that by use of Clapeyron's law and the hypothesis that n does not vary with temperature, relation 4 can be written as

$$P_{HNO_3}(X^0_{HNO_3}, T) = A_0\, e^{(-\Delta h^s_{HNO_3}/(RT))}(X^0_{HNO3})^n \qquad (5)$$

where A_0 is a constant. As detailed for HCl,[13] A_0, $\Delta h^s_{HNO_3}$ and n have been determined from our results by two methods.

(1) We have first fitted the data obtained for each temperature to eq 4. Considering the range of composition measured in ice, HNO_3 is certainly at infinite dilution and n can be considered independent of composition. This hypothesis is confirmed by our data obtained at −15 °C where $\log X_{HNO_3}$ is found to be a linear function of $\log P_{HNO_3}$ (slope $^1/_n$; see Figure 3). The parameter n has also been considered independent of temperature despite the fact that our −8 °C results yield a significantly higher value (3.21) than the other temperatures. In fact, this value, as well as those obtained at −25 and −35 °C, has been calculated with only two partial pressures. Moreover, the low solubility values of profiles 15 and 16 have been obtained with very low P_{HNO_3}. Taking into account analytical errors, this value of 3.21 appears less reliable than the other three and we have chosen to take for n the mean value between −15 and −35 °C, which is 2.30. As explained above, HNO_3 is certainly at infinite dilution in ice so that we expect also $\Delta h^s_{HNO_3}$ to be independent of concentration. We have also made the hypothesis that $\Delta h^s_{HNO_3}$ is not temperature-dependent, and we have calculated its mean value between −8 and −35 °C. The parameters A_0 and $\Delta h^s_{HNO_3}$ were determined from calculated solubilities using $n = 2.30$, which gives

$$\Delta h^s_{HNO_3} = 67.5 \pm 8.9 \text{ kJ/mol}$$

$$A_0 = (5.47 \pm 1.3) \times 10^{26} \text{ Pa}$$

Results are reported in Table 3.

(2) A three-variables least-squares method has also been used to determine simultaneously A_0, $\Delta h^s_{HNO_3}$, and n. Errors on the three parameters were not calculated by this method. Calculations yield $A_0 = 1.32 \times 10^{27}$, $\Delta h^s_{HNO_3} = 68.9$ kJ/mol, and $n = 2.32$. As shown in Table 3, these parameters are in good agreement with those obtained by the first method, since they both provide calculated solubilities within the experimental error of the data (20%).

Since the first method provides the uncertainties of the three parameters, the pressure and temperature dependences for the solubility calculated by the first method will be used further in

$$X^0_{HNO_3} = 2.37 \times 10^{-12}\, e^{(3532.2/T)}(P_{HNO_3})^{1/2.3} \qquad (6)$$

where P_{HNO_3} is the HNO_3 partial pressure in Pa, T is the temperature in Kelvin, and $X^0_{HNO_3}$ is the solubility in mole fraction. Equation 6 has been used to calculate isosolubility curves in the partial pressure versus inverse temperature phase diagram in Figure 4. In the liquid solution domain, isosolubility curves have been determined from the data of Jaecker−Voirol et al.[33] The liquid−solid phase boundary has been determined using the data of Ji and Petit.[21] The ice−trihydrate boundary is from Wooldridge et al.[34] The *solidus* curve has been calculated from the intersection of the solid solution isosolubility lines with the phase boundary, and it is shown in the temperature−composition phase diagram of Figure 5, together with the *liquidus* from Ji and Petit.[21] The partition coefficient K defined at a given temperature as $K = S/L$, where S and L denote, respectively, the solidus and liquidus composition, has also been calculated from our results and Ji and Petit's *liquidus* composition. Results are reported in Figure 6.

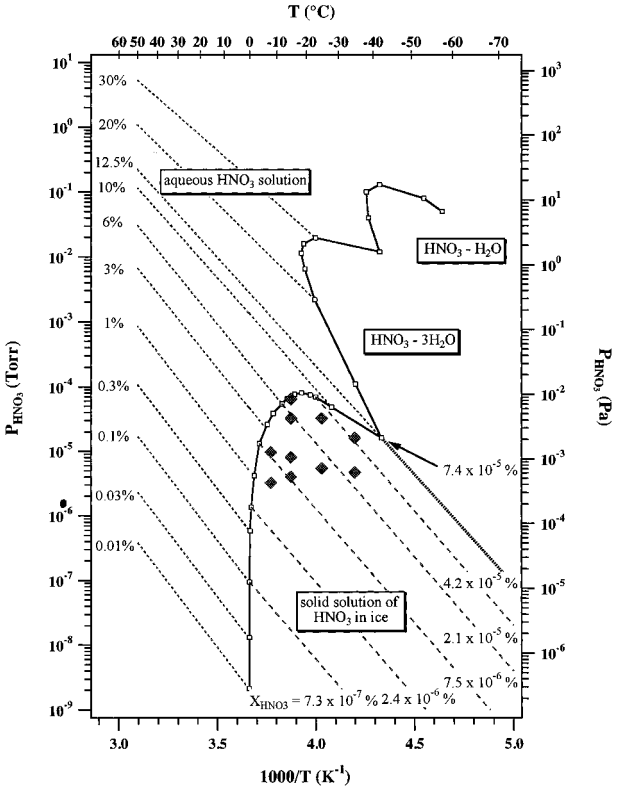

Figure 4. Isosolubility curves in mole fraction for HNO_3 in ice (calculated from eq 6) and in aqueous solutions (calculated from Jaecker-Voirol et al.[33]) as a function of P_{HNO_3} and inverse temperature. The symbol ◆ indicates our experimental conditions. The solid line is the ice−water boundary from Ji and Petit.[21] The dotted line is the ice-trihydrate boundary from Wooldridge et al. 1995.

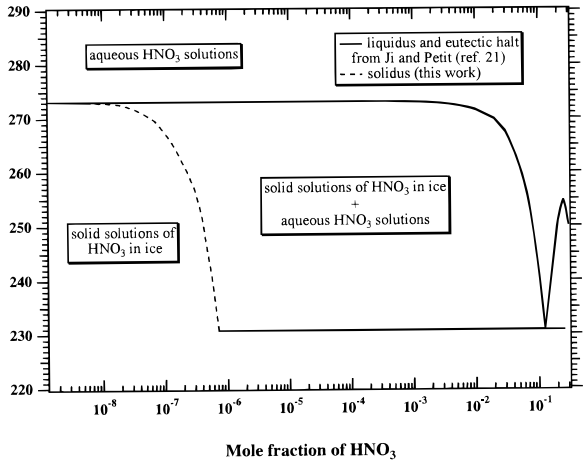

Figure 5. HNO_3−H_2O temperature composition phase diagram (logarithmic scale) at low HNO_3 mole fractions. The dashed line is the *solidus* line calculated from our data.

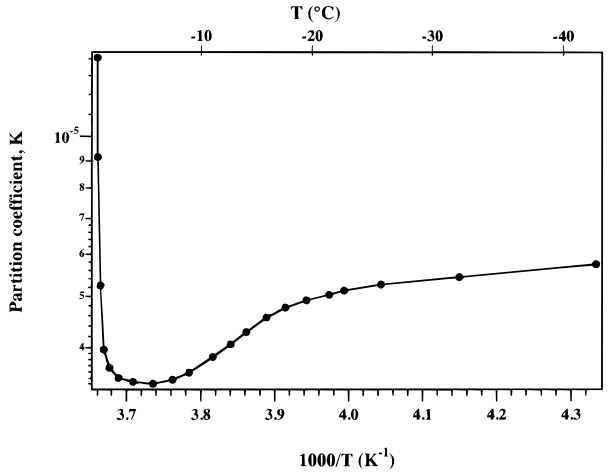

Figure 6. Calculated partition coefficient K versus inverse temperature. Calculations were performed for the points shown. The line joining the points is a visual aid.

IV. Discussion

IV.1. Kinetics. The diffusion coefficient that we have measured for HNO_3 is higher than that found for HCl by a factor of about 100 (ref 13). Because short circuits affect diffusion at long distances, we have only used the first five to seven points of the diffusion profiles to determine D. The classical treatment of diffusion profiles perturbed by short circuits is based on Fisher's model.[35] The volume of short circuits is represented by a volume where the diffusion coefficient is $D' \gg D$. According to Harrison's[36] classification of kinetic regimes of diffusion, our experimental conditions take place in the so-called "B" kinetic regime. Under such conditions, profiles follow Fick's law of diffusion. However, in that case the diffusion coefficient is not the one which occurs in the lattice, D, but instead is the apparent diffusion coefficient, D_{app}, which takes into acount the fraction, τ, of the lattice sites located in short circuits:[37]

$$D_{app} = (1 - \tau)D + \tau D' \qquad (7)$$

Our data obtained for HCl[12,13] suggest that the density and the disorientation of small-angle boundaries vary between samples. D_{app} is then not expected to follow an Ahrrenius law. Figure 1 shows that, even though there is some scatter in the data, D appears to follow an Arrhenius law. The reason may be that because HNO_3 diffuses much more quickly than HCl in ice, the relative effect of the short circuits will be much smaller and therefore less apparent, as suggested by the fact that deviation from eq 2 occurs at deeper distances from the surface in HNO_3 profiles. It then seems reasonable to assume that $D_{app} \approx D$ in the case of HNO_3. Despite the better accuracy of D, we do not see, as for HCl, any significant anisotropy of diffusion. Anisotropy is not necessarily expected, however, because the self-diffusion of H_2O in ice shows little, if any, anisotropy.[32]

The activation energy of diffusion of HNO_3 in ice that we have measured, $E_{diff} = 50$ kJ/mol, is smaller than the value observed for oxygen-18 and tritium in ice, which is 63 kJ/mol.[32] Two mechanisms of diffusion can be considered here: vacancy diffusion and interstitial diffusion.

(1) In the case of the vacancy mechanism, the activation energy of diffusion (50 kJ/mol from our data) is the sum of three terms: the energy required to form a vacancy, the energy of migration of a water molecule between two substitutional sites, and the enthalpy of migration of HNO_3, ΔH^m, between two substitutional sites.[30] The first two energies are equivalent to the activation energy of the self-diffusion vacancy mechanism in ice, which is about 40 kJ/mol at $T < 223$ K.[38] Therefore, the enthalpy of migration, ΔH^m, should be about 10 kJ/mol. This seems weak compared with the enthalpy of migration of water molecules in ice, which is 15.4 kJ/mol.[39]

(2) The interstitial mechanism then appears more reasonable, since vacancies are not involved and the activation energy is equal to the energy of migration, ΔH^m, of HNO_3. Considering the scatter in our diffusion data and the resulting uncertainty of the activation energy of diffusion, this conclusion should be taken as preliminary.

IV.2. Thermodynamics. The solubility of HNO_3 in ice is lower than that of HCl by a factor of about 25 in the (P_{HNO_3}, T) range studied. This is in contrast with aqueous solutions, where the solubility of HNO_3 in water is roughly twice that of HCl. The fact that we have measured a low solubility associated with a high diffusion coefficient may suggest that diffusion has only occurred in short circuits. If the duration of diffusion is too short, diffusion takes place in the "C" regime of diffusion.[36] In that case, diffusion profiles follow eq 2 with the diffusion coefficient D' ($D' \gg D$) of the diffusing element in the short circuits.[30] However, our diffusion profiles for HNO_3 distinctly show two different parts as observed for HCl. This is usually observed when diffusion experiments are performed in the "B" regime where diffusion occurs in both the crystal lattice and in short circuits.

As detailed for HCl,[13] the temperature dependence of the ice/water partition coefficient K of a solute is related to the difference in the number of species created by the solute between the liquid (n_l) and the solid (n_s) and to the difference between the partial molar enthalpies of sublimation and vaporization of the solute according to

$$n_l \frac{d \ln K}{d(1/T)} = \frac{\Delta h^s_{HNO_3} - \Delta h^v_{HNO_3}}{R} + (n_l - n_s) \frac{d \ln S(T)}{d(1/T)} \qquad (8)$$

Figure 6 shows that for HNO_3, K varies with temperature. Because the data of Figure 3 confirm that HNO_3 in ice can be treated as a solute at infinite dilution, it is reasonable to expect that $\Delta h^s_{HNO_3}$ and n_s do not vary with concentration and with temperature in the range considered in Figure 6. We must therefore conclude that, as for HCl, the variations of K with temperature are due to changes in the mode of incorporation of HNO_3 in water as temperature decreases and the HNO_3 concentration increase in the univariant phase boundary. This is not surprising, since the mole fraction of HNO_3 in water in the phase boundary increases from 0.01% to 12.5%, and changes in the environment of HNO_3 in water are necessarily expected.

Regarding the sites of incorporation of HNO_3 in ice, the thermodynamic parameter n in eq 4 represents the number of entities created by HNO_3 in ice. HNO_3 is a strong acid and is expected to be ionically dissociated in the ice volume, as expected for HCl (ref 13) and as suggested by IR data at -62 °C (ref 40), thus creating two entities. If HNO_3 were incorporated in a substitutional site, it would be expected to create defects in ice because of its size. These defects would be counted as entities. A substitutional incorporation of HNO_3 in ice would then lead to an expected high value of n, while we find that n is only 2.3. This may indicate that HNO_3 in ice occupies interstitial sites, as already suggested by the diffusion data.

TABLE 4: Partitioning of HNO_3 between the Ice Volume and the Gas Phase for Contrails and Cirrus Clouds at Given Temperatures and Cloud Ice Contents

cloud type	phase	equilibrium (%)	kinetics (%)
contrail: 220 K, 5 mg/m^3	ice	0.7	9.6
	gas	99.3	90.4
contrail: 220 K, 50 mg/m^3	ice	9.3	62
	gas	90.7	38
cirrus: 238 K, 100 mg/m^3	ice	12	26
	gas	88	74

V. Implications for Cloud Chemistry

The amount of trace gases incorporated in cloud ice is not well-known and is not treated adequately by cloud chemistry models at present.[41] Dominé and Thibert[11] have proposed a mechanism of incorporation of trace gases in ice growing from the gas phase where equilibrium and kinetic processes compete to determine ice composition. Predicting the volume composition of ice from this mechanism requires the knowledge of the gas-phase composition and temperature, the sticking coefficient of the trace gas on the ice surface, the equilibrium solubility and the diffusion coefficient of the trace gas in ice, the growth rate of the ice, and the height of the growth step on the ice surface. The measurements of the diffusion and solubility of HNO_3 in ice will now be used to attempt to predict the partitioning of HNO_3 between the ice volume and the gas phase in cirrus clouds and in condensation trails of airplanes (contrails) according to this mechanism.

V.1. Contrails. Arnold et al.[42] measured gaseous HNO_3 in the upper troposphere and in contrails and found values of 40 and 460 pptv, respectively. This latter value translates into $P_{HNO_3} = 1 \times 10^{-5}$ Pa. Danilin et al.[43] modeled contrail chemistry and obtained a similar value (500 pptv). Assuming a typical upper tropospheric temperature at midlatitudes of 220 K (−53 °C), the saturating vapor pressure of ice is 2.7 Pa.[44] Under these conditions, the solubility of HNO_3 in ice is 1.5×10^{-7} mole fraction. Contrails can have variable condensed water contents, depending on engine characteristics and the age of the contrail. A reasonable range is between 5 and 50 mg of ice per m^3 (ref 45). Table 4 shows the partitioning of HNO_3 assuming that HNO_3 is in equilibrium between the ice and gas phases. Clearly, the volume uptake of HNO_3 by ice is small: less than 10% in both cases.

The uptake of HNO_3 by ice in contrails may not be ruled by equilibrium thermodynamics, however. At 220 K, Figure 1 indicates that $D = 2 \times 10^{-12}$ cm^2/s, and the work of Dominé and Thibert[11] suggests that kinetic effects may well dominate under those conditions. In that case, the ice HNO_3 content will be determined by the relative number of sticking collisions of HNO_3 on the ice surface:

$$X_{HNO_3} = \frac{P_{HNO_3}\alpha_{HNO_3}}{P_{H_2O}\alpha_{H_2O}}\sqrt{\frac{M_{H_2O}}{M_{HNO_3}}} \qquad (9)$$

where α is the sticking coefficient on ice and M the molecular mass. Hanson[46] has found $\alpha_{HNO_3} \geq 0.3$ around 195 K and Abbatt[47] found $\alpha_{HNO_3} \geq 0.2$ around 220K. Haynes et al.[48] have measured $\alpha_{H_2O} = 0.6$ around 220 K. By use of this latter value and $\alpha_{HNO_3} = 0.6$ to account for the fact that α_{HNO_3} measurements are only lower limits, Table 4 shows that if the ice content of the contrail is high enough, most of the HNO_3 will be captured by the ice volume.

The present calculations do not take into account the amount of HNO_3 located on the ice surface. The recent work of Abbatt[47] suggests that a significant fraction of HNO_3 could be located on the ice surface. Because the calculations of Table 4 are based on gas-phase values measured in the atmosphere, the data of Abbatt will not change our relative proportion between the gas phase and the ice volume.

V.2. Cirrus Clouds. Cirrus clouds are usually found between −35 and −60 °C and can have ice contents in the range 50−200 mg of ice per m^3 (refs 45 and 49). To illustrate the incorporation of HNO_3 in clouds in conditions significantly different from those used for contrails, calculations have been performed for a cirrus cloud at an altitude of about 8000 m, where $T = -35$ °C (238 K) and $= 2 \times 10^{-6}$ Pa, with an ice content of 100 mg/m^3. Results for both cases where incorporation is ruled by equilibrium or by kinetics are shown. At −35 °C, D is about 2×10^{-11} cm^2/s, and the incorporation of HNO_3 in ice will probably be between both extremes shown in Table 4. Again, these calculated values do not take into account HNO_3 adsorbed on ice.

VI. Implications for Ice Cores

At present, analyzing ice cores is the only direct method that can potentially yield past HNO_3 atmospheric mixing ratios. Determining past HNO_3 mixing ratios from ice cores requires knowledge of at least (1) the relationship between snow and air composition (air-to-snow transfer function[9,10]), (2) sources other than HNO_3 that contribute to the NO_3^- signal in snow, since HNO_3 in snow is measured by ion chromatography as the nitrate ion, (3) HNO_3 exchanges between the boundary layer and the firn after deposition, and (4) the diffusion of NO_3^- in the ice once the firn porosity has been closed off.

As illustrated for cloud chemistry, the relationship between fresh snow and air compositions will depend on the growth rate of the snow crystal. A detailed discussion of this aspect will be the subject of a future paper. Sources that could contribute to the nitrate signal in snow include ammonium nitrate and calcium nitrate.[50,51] Postdepositional exchanges of HNO_3 are not well understood and would require separate studies.

Diffusion of NO_3^- in ice can be briefly discussed here. Nitrate signals near the surface (i.e., for recent snow layers) often show a clear seasonality[52] that may be smoothed or even disappear if diffusion takes place, resulting in a disruption of the atmospheric signal that must be understood for a correct interpretation. Polar ice at depths greater than 50 m is at about −32 °C in Greenland sites such as Summit, at the top of the ice cap. From eq 3, $D = 2.0 \times 10^{-11}$ cm^2/s at −32 °C, and the migration distance of NO_3^- in ice, taken as $\sqrt{Dt}$, will be 0.8 cm after 1000 years, 4.4 cm after 31 000 years, and 8 cm after 100 000 years. At Summit, simultaneous high-resolution electrical conductivity measurements (which are in fact measurements of the ice acidity, since H^+ is the main charge carrier in ice[53]) and nitrate measurements have been performed on the GRIP ice core (E. Wolff and R. Mulvaney, personnal communication). The data at a depth between 2133.75 and 2134 m, which corresponds to ice about 31 000 year old, show the presence of two types of conditions. The first type is typical glacial conditions, where the ice is alkaline. The second type is milder conditions, where the ice is acidic. In acidic ice, the nitrate concentration is roughly constant around 65 ng/g (i.e., $X_{HNO_3} = 18.9 \times 10^{-9}$), and no seasonality in the nitrate signal is observed, as expected from the diffusion distance of 4.8 cm under those conditions and from the thickness of annual layers, less than 3 cm. When the ice becomes alkaline, however, the nitrate concentration shows seasonal peaks about 1 cm thick or less, with concentrations of about 140 ng/g (i.e., $X_{HNO_3} = 40.6$

$\times 10^{-9}$). Lows are around 60 ng/g. These narrow seasonal peaks suggest that the D value we measured does not apply to the conditions of this part of the ice core.

The explanation may be as follows. In our laboratory ice, HNO_3 is probably dissociated to H^+ and NO_3^-. Thus, in our experiments, diffusion of both these ions will take place, but with different diffusion coefficients, creating an electric field that will affect ion migration and result in the measurement of an effective diffusion coefficient D_{eff} (ref 30):

$$D_{eff} = \frac{D_{H^+} D_{NO_3^-}}{D_{H^+} + D_{NO_3^-}} \quad (10)$$

It is clear that $D_{H^+} \gg D_{NO_3^-}$ so that in our experiment the value we measured is very close to $D_{NO_3^-}$. However, in alkaline ice, the cation associated with NO_3^- is not H^+. In the part of the GRIP ice core discussed here, cations have not been measured with high resolution so far. However, major anions and cations have been measured 50 cm higher in the core, with a spatial resolution coarser than that performed by Wolff and Mulvaney, at a depth around 2133.45 m (refs 54−56, with concentrations around 2133.45 m from Legrand, personal communication). The ice is also alkaline, suggesting that climatic and atmospheric conditions were similar to those of the core 50 cm lower, and a reasonable assumption is that its chemistry should be essentially similar to that of the core analyzed by Wolff and Mulvaney. The main anions are (in ng of ion per gram of ice, with standard deviation of the measurements) NO_3^- (67 ± 21), SO_4^{2-} (53 ± 13), and Cl^- (49 ± 13). Other anions such as formate, acetate, and methanesulfonate are present at less than 6 ng/g. The most important cations are Ca^{2+} (58 ± 14) and Na^+ (25 ± 8). Minor ions are NH_4^+ (3.3 ± 1.6) and Mg^{2+} (6.8 ± 1.2). These analyses clearly show that the cations interacting with NO_3^- in the alkaline ice analyzed by Wolff and Mulvaney are probably essentially Ca^{2+} and Na^+. To our knowledge, the diffusion coefficients of these cations in ice are not known, but it is reasonable to suggest that they will be much lower than that of the highly mobile H^+. This will probably result in an effective diffusion coefficient of NO_3^- much smaller than what we measured in our simplified chemical system, and this may have preserved the seasonality of the nitrate signals in alkaline ice. Thus, interactions between ions during their diffusion in ice must be studied before diffusion of ions in polar ice can be understood.

VII. Summary and Conclusion

The diffusion coefficient and equilibrium solubility of HNO_3 in ice have been measured between −8 and −35 °C. HNO_3 is about 25 times less soluble in ice than HCl. This may be due in part to its larger size. HNO_3 diffuses much more quickly than HCl in ice. Probably because of this fast diffusion, the effect of small-angle boundaries that act as diffusion short circuits is relatively less important than for HCl, and the diffusion coefficients measured here are probably accurate within a factor of 3. At −35 °C, D is probably close to 1×10^{-11} cm^2/s, while at −8 °C, D is probably around 2×10^{-10} cm^2/s. Because of this fast diffusion, the incorporation of HNO_3 in ice growing from the gas phase in clouds at $T > -40$ °C may have a significant contribution from equilibrium processes. It is found that although ice clouds can scavenge most of the HCl present in their air mass, under most conditions a large part of the HNO_3 will remain in the air mass of the cloud. This conclusion does not take into account surface processes. If surface processes are as important as suggested by Abbatt's experimental work,[47] then most of the HNO_3 will be taken up by ice, either by its surface or in its volume. The comparison of ice core data with our laboratory measurements illustrates the point that ions interact during their diffusion in ice and that the diffusion coefficient that we measured here is valid when H^+ is the cation associated with NO_3^-. If heavier ions, such as Ca^{2+} and Na^+, which will doubtless diffuse much more slowly than H^+, are associated with NO_3^-, then the diffusion coefficient of NO_3^- in ice may be orders of magnitude slower.

Acknowledgment. This work was supported by the Commission of the European Community (Contract EV5V-CT93-0336), CNRS (PAMOY and Avion-ozone programs), Région Rhône-Alpes, and Université Joseph Fourier of Grenoble. We thank Eric Wolff and Robert Mulvaney, British Antarctic Survey, for kindly communicating their Summit ice core data prior to publication, and our colleague Michel Legrand for communicating detailed analyses of the GRIP ice core.

References and Notes

(1) Bricker, O. P.; Rice K. C. *Annu. Rev. Earth Planet. Sci.* **1993**, *21*, 151.
(2) Leighton, P. A. *Photochemistry of air pollution*; Academic Press: New York, 1961.
(3) Solomon, S.; Garcia, R. R.; Rowland, F. S.; Wuebbles, D. J. *Nature* **1986**, *321*, 755.
(4) Logan, J. A. *J. Geophys. Res.* **1983**, *88*, 10785.
(5) Ehhalt, D. H.; Drummond, J. W. In *Chemistry of the unpolluted and polluted troposphere*; Georgü, H. W., Jaeschke, W., Eds.; NATO ASI Series, C96; Reidel: Dordrecht, 1982; pp 219−251.
(6) McElroy, M. B.; Elkins, J. W.; Wofsy, S. C.; Yung, Y. L. *Rev. Geophys. Space Phys.* **1976,** *14*, 143.
(7) Silvente, E.; Legrand, M. In *Ice core studies of global biogechemical cycles;* Delmas, R. J. Ed.; NATO ASI Series I30; Springer-Verlag: Berlin, 1995; 225−240.
(8) Legrand, M.; Delmas, R. *Tellus* **1986**, *38*, 236.
(9) Legrand, M.; Léopold, A.; Dominé, F. In *Chemical exchange between the atmosphere and polar snow*; Wolff, E., Bales, R. C., Eds.; NATO ASI Series I43; Springer: Berlin, 1996; pp 19−44.
(10) Dominé, F.; Thibert, E.; Silvente, E.; Legrand, M.; Jaffrezo, J.-L. *J. Atmos. Chem.* **1995**, *21*, 165.
(11) Dominé, F.; Thibert, E. *Geophys. Res. Lett.* **1996**, *23*, 3627.
(12) Dominé, F.; Thibert, E.; Van Landeghem, F.; Silvente, E.; Wagnon, P. *Geophys. Res. Lett.* **1994**, *21*, 601.
(13) Thibert, E.; Dominé, F. *J. Phys. Chem. B* **1997**, *101*, 3554.
(14) Pickering, S. U. *J. Chem. Soc.* **1893**, *63*, 436.
(15) Kuster, H.; Kremann R. *Z. Anorg. Chem.* **1904**, *41*, 1.
(16) Biltz, W.; Hülsmann, O.; Eickholtz, W. *Nachr. Gotting. Ges.* **1935**, *2* (1), 99.
(17) Potier, J.; Potier, A. *C.R. Acad. Sci.* **1956**, 1474.
(18) Hanson, D. R.; Mauersberger, K. *J. Phys. Chem.* **1988**, *92*, 6167.
(19) Turco, R. P.; Toon, O. B.; Hamill, P. *J. Geophys. Res.* **1989**, *94*, 16493.
(20) Worsnop, D. R.; Fox, L. E.; Zahniser, M. S.; Wofsy, S. C. *Science* **1993**, *259*, 71.
(21) Ji, K.; Petit, J. C. *C.R. Acad. Sci., Ser. II* **1993**, *316*, 1743.
(22) Tolbert, M. A.; Middelbrook, A. M. *J. Geophys. Res.* **1990**, *95*, 22423.
(23) Ritzhaupt, G.; Devlin, J. P. *J. Phys. Chem.* **1991**, *95*, 90.
(24) Koehler, B. G.; Middelbrook, A. M.; Tolbert, M. A. *J. Geophys. Res.* **1992**, *97*, 8065.
(25) Laird, S. K.; Sommerfeld, R. A. *Geophys. Res. Lett.* **1995**, *22*, 921.
(26) Dominé, F.; Thibert, E. In *Biogeochemistry of seasonally snow-covered catchments*; Tonnenssen, K., Williams, M., Tranter, M., Eds.; IAHS Publication 228; IAHS Press: Wallingford, U.K., 1995; pp 3−10.
(27) Dominé, F.; Chaix, L.; Thibert, E. Air pollution research report 56, Polar srtatospheric ozone. *Proceedings of the 3rd European Workshop, Shliersee, Germany*; European Community: Luxembourg, 1996; pp 736−739.
(28) Pascal, P. *Nouveau traité de chimie minérale*; Masson et C^{ie}: Paris, 1960; Volume XVI.
(29) Burkholder, J. B.; Talukdar, R. K.; Ravishankara, A. R.; Solomon, S. *J. Geophys. Res.* **1993**, *98*, 22937.
(30) Philibert, J. *Diffusion et transport de matière dans les solides*; Les éditions de physique: Les Ulis, France, 1990; Chapter I.
(31) Badrour, L.; Moya, E. G.; Bernardini, J.; Moya, F. *J. Phys. Chem. Solids* **1989**, *50*, 551.
(32) Hobbs, P. V. *Ice Physics*; Clarendon Press: Oxford, U.K., 1974.

(33) Jaecker-Voirol, A.; Ponche, J. L.; Mirabel, P. *J. Geophys. Res.* **1990**, *95*, 11857.
(34) Wooldridge, P. J.; Zhang, R.; Molina, M. J. *J. Geophys. Res.* **1995,** *100*, 1389.
(35) Fisher, J. C. *J. Appl. Phys.* **1951**, *22*, 74.
(36) Harrison, H. *Science* **1970**, *170*, 734.
(37) Hart, E. W. *Acta Metall.* **1957**, *5*, 597.
(38) Eldrup, M. *J. Chem. Phys.* **1976**, *64*, 5283.
(39) Hondoh, T.; Azuma, K.; Higashi, A. *J. Phys.* **1987**, *48*, C1−C183.
(40) Zondlo, M. A.; Barone, S. B.; Tolbert, M. A. *Geophys. Res. Lett.* **1997**, *24*, 1391.
(41) Audiffren, N.; Cautenet, S. *J. Applied Meteorol.*, in press.
(42) Arnold, F.; Scheidt, J.; Stilp, T.; Schlager, H.; Reinhardt, M. E. *Geophys. Res. Lett.* **1992**, *19*, 2421.
(43) Danilin, M. Y.; Ebel, A.; Elbern, H.; Petry, H. *J. Geophys. Res.* **1994**, *99*, 18951.
(44) Marti, J.; Mauersberger, K. *Geophys. Res. Lett.* **1993**, *20*, 363.
(45) Gayet, J. F.; Febvre, G.; Brogniez, G.; Chepfer, H.; Renger, W.; Wendling, P. *J. Atmos. Sci.* **1996**, *53*, 126.
(46) Hanson, D. R. *Geophys. Res. Lett.* **1992**, *19*, 2063.
(47) Abbatt, J. P. D. *Geophys. Res. Lett.* **1997**, *24*, 1479.
(48) Haynes, D. R.; Tro, N. J.; George, S. M. *J. Phys. Chem.* **1992**, *96*, 8502.
(49) Heymsfield, A. J.; Knollenberg, R. G. *J. Atmos. Sci.* **1972**, *29*, 1358.
(50) Wolff., E. In *Ice core studies of global biogeochemical cycles;* Delmas, R. Ed.; NATO ASI Series 30; Springer-Verlag: New York, 1995; p 224.
(51) Legrand, M.; Mayewski, P. *Rev. Geophys.* **1997**, *35*, 219.
(52) Mayewski, P. A.; Legrand, M. *Nature* **1990**, *346*, 258.
(53) Hammer, C. U. *J. Glaciol.* **1980**, *25*, 359.
(54) Legrand, M.; De Angelis, M. *J. Geophys. Res.* **1996**, *101*, 4129.
(55) Fuhrer, K.; Neftel, A.; Ankin, M.; Staffelbach, T.; Legrand, M. *J. Geophys. Res.* **1996**, *101*, 4147.
(56) Legrand, M.; Hammer, C.; De Angelis, M.; Savarino, J.; Delmas, R.; Clausen, H.; Johnsen, S. J. *J. Geophys. Res.* **1997,** *102*, 26663.